JOURNAL OF SYNCHROTRON RADIATION

ISSN 1600-5775

XANES reflects coordination change and underlying surface disorder of zinc adsorbed to silica

Joey Nelson*

School of Earth, Energy and Environmental Sciences, Stanford University, 450 Serra Mall, Stanford, CA 94305-2115, USA, and Office of the Vice Provost for Undergraduate Education, Stanford University, 590 Escondido Mall, Stanford, CA 94305-3068, USA. *Correspondence e-mail: joey.nelson@stanford.edu

Received 20 January 2021
Accepted 15 April 2021

Edited by K. Kvashnina, ESRF – The European Synchrotron, France

Keywords: zinc; adsorption; silica; surface disorder; XANES spectroscopy.

Supporting information: this article has supporting information at journals.iucr.org/s

Zinc *K*-edge X-ray absorption near-edge structure (XANES) spectroscopy of Zn adsorbed to silica and Zn-bearing minerals, salts and solutions was conducted to explore how XANES spectra reflect coordination environment and disorder in the surface to which a metal ion is sorbed. Specifically, XANES spectra for five distinct Zn adsorption complexes (Zn_{ads}) on quartz and amorphous silica [$SiO_{2(am)}$] are presented from the Zn–water–silica surface system: outer-sphere octahedral Zn_{ads} on quartz, inner-sphere octahedral Zn_{ads} on quartz, inner-sphere tetrahedral Zn_{ads} on quartz, inner-sphere octahedral Zn_{ads} on $SiO_{2(am)}$ and inner-sphere tetrahedral Zn_{ads} on $SiO_{2(am)}$. XANES spectral analysis of these complexes on quartz versus $SiO_{2(am)}$ reveals that normalized peak absorbance and *K*-edge energy position generally decrease with increasing surface disorder and decreasing Zn–O coordination. On quartz, the absorption-edge energy of Zn_{ads} ranges from 9663.0 to 9664.1 eV for samples dominated by tetrahedrally versus octahedrally coordinated species, respectively. On $SiO_{2(am)}$, the absorption-edge energy of Zn_{ads} ranges from 9662.3 to 9663.4 eV for samples dominated by tetrahedrally versus octahedrally coordinated species, respectively. On both silica substrates, octahedral Zn_{ads} presents a single *K*-edge peak feature, whereas tetrahedral Zn_{ads} presents two absorbance features. The energy space between the two absorbance peak features of the XANES *K*-edge of tetrahedral Zn_{ads} is 2.4 eV for Zn on quartz and 3.2 eV for Zn on $SiO_{2(am)}$. Linear combination fitting of samples with a mixture of Zn_{ads} complex types demonstrates that the XANES spectra of octahedral and tetrahedral Zn_{ads} on silica are distinct enough for quantitative identification. These results suggest caution when deciphering Zn speciation in natural samples via linear combination approaches using a single Zn_{ads} standard to represent sorption on a particular mineral surface. Correlation between XANES spectral features and prior extended X-ray absorption fine structure (EXAFS) derived coordination environments for these Zn_{ads} on silica samples provides insight into Zn speciation in natural systems with XANES compatible Zn concentrations too low for EXAFS analysis.

1. Introduction

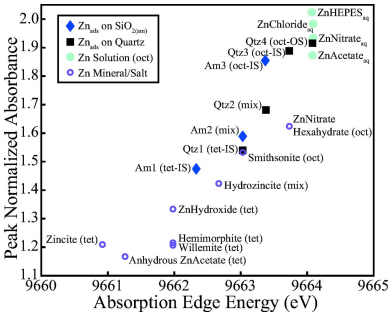

Zinc serves as a micronutrient or toxicant to nearly all life forms depending on concentration and coordination (Sandstead, 2014). Identifying the chemical speciation of Zn facilitates better prediction of its reactivity, fate and transport through the environment, where partitioning of Zn onto natural surfaces may lead to spatial heterogeneity and thus mitigate bioavailability. Sorption of Zn to complex and variably ordered mineral interfaces can be an important reservoir in a wide array of natural systems from aquifer sands (Coston *et al.*, 1995) to the silica frustules of diatoms (Ellwood & Hunter, 2000). Therefore, investigation of sorption complexes with methodologies that employ rapid identification of mole-

cular-level Zn complexes at environmentally relevant concentrations, sometimes yielding low surface coverage, enables the collection of key insights into Zn biogeochemistry.

The propensity for transition metals, including Zn, to reside in multiple coordination environments makes aqueous, sorbed and mineral speciation complex and identification in unknown specimens challenging. Such variations in the Zn coordination environment have been documented at several mineral surfaces, including silica (Nelson *et al.*, 2017, 2018; Roberts *et al.*, 2003), kaolinite (Guinoiseau *et al.*, 2016; Nachtegaal & Sparks, 2004), alumina (Trainor *et al.*, 2000; Roberts *et al.*, 2003), montmorillonite (Lee *et al.*, 2004), birnessite (Qin *et al.*, 2018; Manceau *et al.*, 2002), hematite (Ha *et al.*, 2009), goethite (Nachtegaal & Sparks, 2004; Hamilton *et al.*, 2016) and ferrihydrite (Waychunas *et al.*, 2002). The precise bonding environment of Zn on mineral surfaces has implications for mobility and toxicity because different sorbed species may be differentially labile, such as octahedral versus tetrahedral Zn complexes on birnessite (Qin *et al.*, 2018) and inner-sphere versus outer-sphere Zn complexes on hematite (Ha *et al.*, 2009). Commonly, the molecular environment of Zn in natural samples, especially in non-crystalline phases such as protein-bound and surface-sorbed species, has been probed with the extended X-ray absorption fine structure (EXAFS) region of X-ray absorption spectroscopy (XAS). With more detailed investigation of diagnostic features in Zn *K*-edge X-ray absorption near-edge structure (XANES) spectra correlated to characteristics of the Zn coordination environment and geometry, XANES analysis may further aid probing of Zn speciation at substantially lower concentrations compared with those required for EXAFS analysis.

Zn *K*-edge XANES analysis has been used in studies of catalysts (Schweitzer *et al.*, 2014), anthropological examination of cultural materials (Veiga & Figueiredo, 2008), speciation in aqueous fluid environments and organic solvents (Migliorati *et al.*, 2012), ligation in model microorganisms (Thomas *et al.*, 2019), identification of target treatments for cancer cells by a relationship with the transition-metal oxidation state (Al-Ebraheem *et al.*, 2010), and distribution and association in soil samples to sewer sludge via linear combination fitting (LCF) of XANES spectra (Mamindy-Pajany *et al.*, 2014; Martínez *et al.*, 2006; Rouff *et al.*, 2013; Hamilton *et al.*, 2016). Importantly, Castorina *et al.* (2019) characterized the Zn *K*-edge XANES spectra of a suite of Zn mineral and organic standards to support the future application of linear combination approaches in identifying unknown mixtures. The set of Zn mineral and organic standards shows little spectral variation as a result of natural variation in natural mineral standards and elucidates that differences in leading-edge position and post-edge peak height can be attributed to differences in Zn coordination (Castorina *et al.*, 2019). Similar characterization of Zn adsorption complexes (Zn_{ads}) at mineral surfaces may be of similar benefit yet remains to be extensively conducted, in part due to increased difficulty in preparing replicable Zn adsorption samples and the unknown molecular adsorption geometries of many such complexes on various mineral surfaces. For example, the inner-sphere adsorption of Zn to mineral–water interfaces may occur via release of one or more waters of hydration and bonding to any one of multiple adsorption sites with differing surface functionality (*e.g.* hydroxylated, deprotonated, adsorbed onto by a different cation) depending on the underlying mineral surface, Zn concentration and chemical conditions of the aqueous environment.

Despite the variability in Zn_{ads} at mineral surfaces, use of a single sample to represent sorbed Zn phases on a mineral surface in LCF of natural samples is not uncommon [*e.g.* Zn on goethite (Hamilton *et al.*, 2016; Mamindy-Pajany *et al.*, 2014)]. Additionally, systematic exploration of Zn adsorption complexes with XANES is sparse due to the infrequency of Zn to take on multiple oxidation states within a single natural sample and the assumed inability of XANES analysis to independently ascertain molecular geometries (Waychunas *et al.*, 2003). When systematic EXAFS analysis has been undertaken on such complexes at mineral–water interfaces, the strength and depth of molecular-level findings have often been presented without direct correlation with what may be represented in the XANES region of X-ray absorption spectra. However, identification of such correlations may be of practical use for XAS-based inquiry in Zn studies at low surface coverage and environmentally relevant concentrations. Such identification is also needed to ensure appropriate Zn adsorption standards are employed when using linear combination approaches to determine Zn partitioning in natural samples, often containing complex mineral assemblages with variably disordered surfaces to which transition-metal ions may sorb.

This article systematically examines the impact of the local coordination environment on Zn *K*-edge XANES spectra where EXAFS and surface complexation modeling investigation have previously elucidated the dominant molecular geometry of Zn complexes on silica surfaces. While EXAFS spectral regions are generally insensitive to the second solvation shell around an aqueous metal ion, the XANES region is at times impacted by the interactions of solvation shells beyond the first (Migliorati *et al.*, 2012). Moreover, EXAFS analysis of Zn adsorbed to quartz versus amorphous silica [$SiO_{2(am)}$] (Nelson *et al.*, 2017) and microparticulate versus nanoparticulate hematite (Ha *et al.*, 2009, 2007) indicates that underlying mineral surface disorder (*i.e.* degree of crystallinity) affects adsorption complex geometry. Surface disorder effects on adsorption complexes are thus expected to manifest in XANES spectra. This study interrogates such variability with *K*-edge XANES analysis of Zn_{ads} on quartz and $SiO_{2(am)}$. The modeling of such complexes may be complicated by asymmetry in the sorbed structures, varying degrees of disorder in the underlying surface that may impact spectral features and instantaneously changing solvation within the near-surface environment. The degrees to which such complexities must be considered in spectral calculations and in the generation of starting models may be informed by the experimental examination presented here. This Zn *K*-edge XANES spectral analysis of Zn-bearing minerals, solutions and adsorption complexes on silica provides insight into where

XANES spectral analysis is useful in interrogating metal-ion coordination at the mineral–water interface and at concentrations too low for EXAFS spectral analysis.

2. Materials and methods

The Zn-bearing mineral standards presented here were previously characterized by EXAFS and X-ray diffraction analysis to establish purity and homogeneity of the phases as detailed by Nelson *et al.* (2017). The adsorption samples of Zn on silica presented here were also previously characterized by EXAFS analysis to establish the coordination environment as detailed by Nelson *et al.* (2017). The specific silica substrates were purchased as 0.5–10 µm conchoidally fractured quartz particles and 74–125 µm conchoidally fractured $SiO_{2(am)}$ particles with measured specific surface areas of 5.92 ± 0.06 $m^2\ g^{-1}$ (2σ) and 9.76 ± 0.29 $m^2\ g^{-1}$ (2σ), respectively (Nelson *et al.*, 2017). Adsorption experiments were conducted in ambient laboratory atmosphere at room temperature (22°C). Adsorption batches were made gravimetrically in acid-washed low-density polyethylene bottles. Each batch contained an amount of quartz or $SiO_{2(am)}$ such that the ratio of absolute substrate surface area to fluid was 0.5 m^2 substrate surface area per 1 ml of Zn nitrate solution with or without an added background electrolyte of sodium nitrate to yield an ionic strength of 0.1 *M* or 0.004 *M*, respectively. After a four- to six-day equilibration period at an initial pH of less than 5 on an orbital shaker table, the pH of each batch was adjusted to yield a desired level of Zn surface coverage with a 48-hour equilibration period on an orbital shaker table. Solid-phase samples with adsorbed Zn were obtained for synchrotron-based spectroscopic analyses by transferring the entirety of the batch to a centrifuge tube, centrifuging the entire batch, decanting the solution phase and collecting the solid phase. Resultant levels of Zn surface coverage on silica substrates were determined from triplicate inductively coupled plasma optical-emission spectrometry (ICP-OES) measurement of Zn concentration in initial and decanted solutions. Further conditions of batch reactor experiments, levels of resultant Zn surface coverage and dominant adsorption complex based on prior EXAFS analysis of adsorption samples examined here are summarized in Table 1 [see Nelson *et al.* (2017) for further methodological details of generation, and EXAFS analysis of Zn standards and adsorption samples].

Mineral standards, Zn nitrate salt and Zn acetate salt were individually ground to fine powders, sieved to grain sizes small enough to minimize self-absorption and sprinkled in a homogeneous thin layer onto Kapton tape affixed to open slots in an aluminium sample holder. Adsorption samples were loaded onto slots in aluminium sample holders immediately after extraction from batch reactors. The level of Zn surface coverage in all the adsorption samples presented here was less than 4 µmol m^{-2} (Table 1), which is equivalent to less than 40 µmol of Zn per 1 g of silica and is a low enough density of adsorbed Zn in material loaded onto sample holders so as to avoid the impact of self-absorption. The Zn-bearing solutions examined here were made from dissolving Zn salts in ultra-pure MilliQ water to yield solutions that were loaded onto slots in aluminium sample holders between Kapton tape. Zn *K*-edge XANES spectra were collected at the Stanford Synchrotron Radiation Lightsource (SSRL) on BL 11-2 and BL 4-1 for Zn-bearing solutions (150 m*M* Zn nitrate, 150 m*M* Zn acetate, 150 m*M* Zn chloride, 1 *M* Zn HEPES buffer), Zn-bearing mineral and salt standards [willemite Zn_2SiO_4, hemimorphite $Zn_4Si_2O_7(OH)_3H_3O$, smithsonite $ZnCO_3$, hydrozincite $Zn_3(OH)_6(CO_3)_2$, zincite ZnO, zinc hydroxide $Zn(OH)_2$, zinc nitrate hexahydrate $Zn(NO_3)_2\ 6(H_2O)$, anhydrous zinc acetate $Zn(CH_3CO_2)_2$], and Zn_{ads} on quartz and $SiO_{2(am)}$. The beamline energy was calibrated with a Zn reference foil where the first inflection point was set at the *K*-edge energy of 9659.0 eV. Fluorescence spectra were recorded with a multi-channel Ge detector using a Si(220) double-crystal monochromator detuned 30–35% for rejection of harmonics. A minimum of three spectra was collected for each sample, with a step size of 0.35 eV and a dwell time of 1 s over the XANES region. Spectra were averaged and background subtracted with a spline fitting function in *SIXPack* (Webb, 2005). Normalized absorbance of Zn XANES spectra is presented from 9640 to 9720 eV for Zn mineral and salt standards (Fig. 1), Zn-bearing solutions (Fig. 2), Zn adsorbed to quartz (samples Qtz1, Qtz2, Qtz3 and Qtz4) (Fig. 3), and Zn adsorbed to $SiO_{2(am)}$ (samples Am1, Am2 and Am3) (Fig. 4). All of these Zn XANES spectra (normalized absorbance versus energy) are present in the supporting information for use by others.

Table 1
Zn adsorption sample parameters.

Sample	Substrate	Ionic strength (*M*)	Coverage (µmol m^{-2})	pH	Dominant Zn_{ads} geometry, code†
Am1	$SiO_{2(am)}$	0.004	1.80	7.72	Tet-IS, Q
Am2	$SiO_{2(am)}$	0.004	3.64	7.03	Mix, U
Am3	$SiO_{2(am)}$	0.004	0.21	6.29	Oct-IS, M
Qtz1	Quartz	0.1	0.48	6.96	Tet-IS, H
Qtz2	Quartz	0.004	1.02	7.39	Mix, D
Qtz3	Quartz	0.1	0.15	6.35	Oct-IS, E
Qtz4	Quartz	0.004	0.57	6.50	Oct-OS, B

† Tetrahedral (tet), octahedral (oct), mixture (mix), inner sphere (IS) and outer sphere (OS) based on prior EXAFS spectral analysis for corresponding sample letter code by Nelson *et al.* (2017).

Zn adsorption samples Qtz1, Qtz3 and Qtz4 are each dominated by a single different type of adsorption complex based on prior EXAFS analysis by Nelson *et al.* (2017). Taken together, these samples represent the full set of lone Zn adsorption complexes on quartz that have been documented to date at circumneutral pH and surface coverage below 4 µmol m^{-2} (Table 1). Similarly, Zn adsorption samples Am1 and Am3 represent those found on $SiO_{2(am)}$ (Table 1). As such, these adsorption samples will be referred to here as endmember adsorption complexes for Zn on silica at circumneutral pH. Adsorption samples Am2 and Qtz2 containing mixtures of Zn adsorption complexes (Table 1) were examined to determine if different Zn adsorption complexes on silica are distinct enough for quantitative

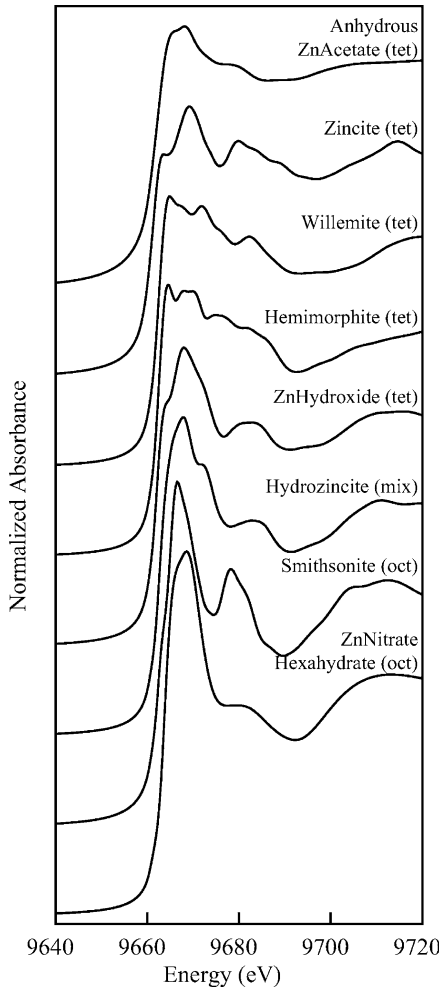

Figure 1
XANES of Zn-bearing minerals and salts. The spectra labels contain an indicator of the Zn coordination environment by O as tetrahedral (tet), octahedral (oct) or a combination of the two (mix).

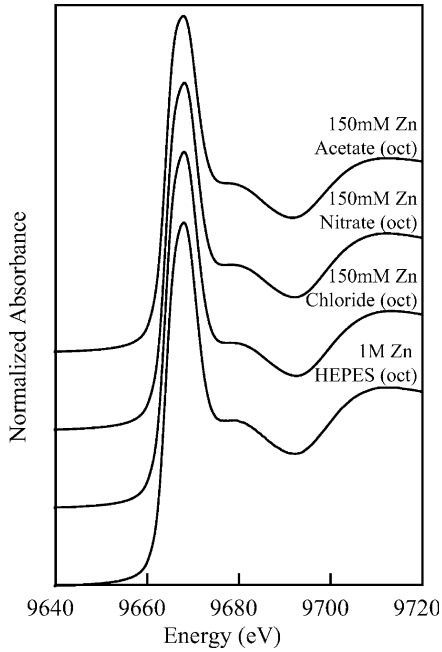

Figure 2
XANES of aqueous standards. The spectra labels contain an indicator of the Zn coordination environment by O.

identification in a mixture, and thus probe whether a single adsorption sample may be reliably used to represent Zn_{ads} on silica in LCF of natural samples. Specifically, these mixture samples host Zn in both octahedral and tetrahedral coordination by O in inner-sphere complexes on quartz and $SiO_{2(am)}$, as well as Zn in both outer-sphere and inner-sphere complexes on quartz. LCF of the XANES spectra of Qtz2 and Am2 by related adsorption complex endmember sample XANES spectra was conducted in *ATHENA* XAS data-processing

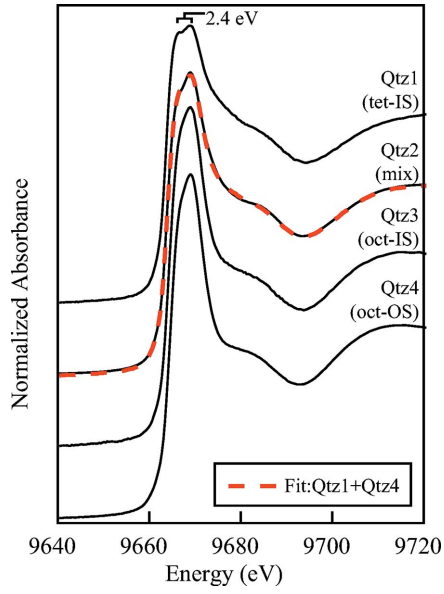

Figure 3
XANES of Zn adsorbed to quartz. The spectra labels contain an indicator of the dominant Zn adsorption complex in the sample as determined by shell-by-shell fitting of EXAFS spectra by Nelson *et al.* (2017): tetrahedral (tet), octahedral (oct), mixture (mix), inner sphere (IS) and outer sphere (OS).

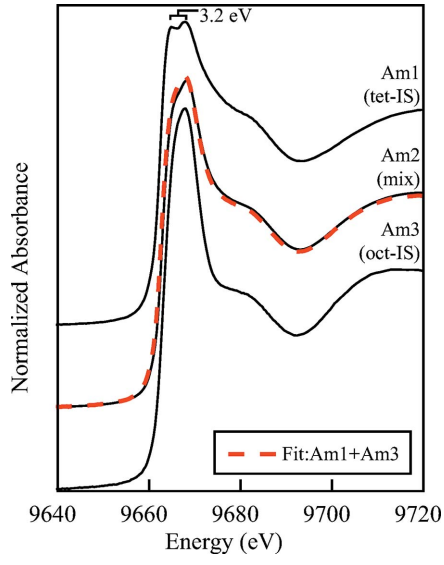

Figure 4
XANES of Zn adsorbed to amorphous silica [$SiO_{2(am)}$]. The spectra labels contain an indicator of the dominant Zn adsorption complex in the sample as determined by shell-by-shell fitting of EXAFS spectra by Nelson *et al.* (2017).

Table 2
XANES LCF.

Sample	Standard 1	Proportion	Standard 2	Proportion	Standard 3	Proportion	Sum of props	*R* factor	Reduced chi-squared
Am2 (mix)	Am1 (tet-IS)	0.527 (0.018)	Am3 (oct-IS)	0.449 (0.018)			0.976	2.71×10^{-3}	7.06×10^{-4}
Qtz2 (mix)	Qtz1 (tet-IS)	0.656 (0.015)	Qtz3 (oct-IS)	0.082 (0.071)	Qtz4 (oct-OS)	0.264 (0.059)	1.002	2.17×10^{-4}	6.00×10^{-5}
	Qtz1 (tet-IS)	0.672 (0.006)			Qtz4 (oct-OS)	0.332 (0.005)	1.004	2.19×10^{-4}	6.01×10^{-5}
	Qtz1 (tet-IS)	0.595 (0.007)	Qtz3 (oct-IS)	0.400 (0.007)			0.995	2.44×10^{-4}	6.69×10^{-5}

software (Ravel & Newville, 2005) (Table 2 and Fig. S1 of the supporting information). The sum of components used in LCF was not forced to unity because no substantial change in fit was observed when this constraint was employed. Errors (1 sd) on proportions of phases used as standards for LCF are noted in the parentheticals of Table 2. Specifically, LCF of Am2 used Am1 [tetrahedral, inner-sphere Zn_{ads} on $SiO_{2(am)}$] and Am3 [octahedral, inner-sphere Zn_{ads} on $SiO_{2(am)}$] as standards. Furthermore, the fitting of mixture sample Qtz2 employed combinations of Qtz1 (tetrahedral, inner-sphere Zn_{ads} on quartz), Qtz3 (octahedral, inner-sphere Zn_{ads} on quartz) and Qtz4 (octahedral, outer-sphere Zn_{ads} on quartz) as standards.

As the ingrowth of a second peak feature in the *K*-edge of the XANES spectra of adsorption samples appears visually distinct from the main peak feature only in samples dominated by tetrahedral coordination (Figs. 3 and 4), a practical plotting strategy was employed following the work of Thomas *et al.* (2019): maximum absorbance in the XANES spectrum, here used to identify the *K*-edge peak height, is plotted against the absorption-edge energy, defined as the energy at one-half the maximum absorbance height in the leading edge of the main peak (Fig. 5). In all samples examined, the absorption-edge energy based on the position of half the peak absorbance is extremely close, if not identical, to that based on the inflection point (determined by taking the maximum of the first derivate) of XANES spectra across the *K*-edge (Fig. S2 and Table S1 of the supporting information). Use of the former (half peak energy) is preferred and presented here over the absorption-edge inflection point (E_0) because of the nature of the smithsonite *K*-edge, which contains two significant and distinct inflection points of similar intensity, unlike all other samples examined here that have a single *K*-edge inflection point (Fig. S2 and Table S1).

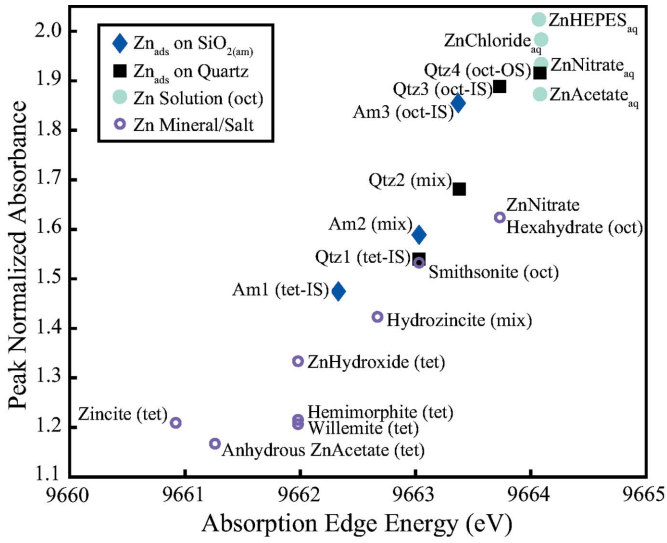

Figure 5
Zn *K*-edge XANES spectra peak normalized absorbance versus absorption-edge energy. The sample and standard labels contain an indicator of the dominant Zn coordination environment.

3. Results and discussion

3.1. Zn-bearing minerals and solutions

Generally, the Zn *K*-edge XANES absorption-edge position is shifted to lower energy in tetrahedrally coordinated Zn–O environments compared with those in octahedral Zn–O environments (Figs. 1, 2 and 5), as observed in the XANES model calculations of Waychunas *et al.* (2003). The normalized absorbance peak intensity of Zn *K*-edge XANES is smaller for Zn mineral and salt standards where Zn is in a first shell coordination with fewer O atoms (Fig. 1). Specifically, absorbance peak intensity for tetrahedrally coordinated Zn solids is less than that of octahedrally coordinated Zn solids, with absorbance peak intensity of minerals containing both coordination environments residing between (Fig. 1). The normalized absorbance peak intensity of Zn *K*-edge XANES is smaller for Zn in more motion-restricted solid form over that in the aqueous phase (compare Fig. 1 with Fig. 2), wherein aqueous Zn (Zn_{aq}) persists predominantly as a single octahedral aquo complex in solutions with ionic strength up to 1 *M* under ambient laboratory conditions (Brugger *et al.*, 2016). As a direct comparison under similar Zn–O coordination environments, the *K*-edge XANES absorbance peak intensity is lower for Zn in Zn nitrate hexahydrate salt than in 150 m*M* of Zn nitrate solution (compare Fig. 1 with Fig. 2). These observations corroborate prior findings for Zn-bearing minerals and solutions (Castorina *et al.*, 2019; Thomas *et al.*, 2019; Waychunas *et al.*, 2003; Hamilton *et al.*, 2016; Bazin *et al.*, 2009), and expand the set of documented Zn *K*-edge XANES spectral standards.

3.2. Zn_{ads} on silica

The type of Zn adsorption complex(es) formed on the surface of silica in aqueous environments depends on ionic strength and Zn surface coverage as determined by pH and

the concentration of Zn relative to the amount of available reactive mineral surface area (Nelson *et al.*, 2017, 2018; Roberts *et al.*, 2003; Anderson & Benjamin, 1990; Osaki *et al.*, 1990; Sverjensky, 1993; Davis *et al.*, 1998; Liu *et al.*, 2003). At circumneutral pH, ionic strength less than 1 *M* and Zn surface coverage less than 4 μmol m^{-2}, quartz bears outer-sphere and inner-sphere Zn complexes, whereas $SiO_{2(am)}$ hosts only inner-sphere Zn complexes (Nelson *et al.*, 2017, 2018; Roberts *et al.*, 2003). Specifically, the silica substrates used here present inner-sphere tetrahedral (tet-IS), inner-sphere octahedral (oct-IS) and outer-sphere octahedral (oct-OS) complexes on quartz, and tet-IS and oct-IS complexes on $SiO_{2(am)}$ (Table 1). The Zn adsorption samples herein represent these five endmembers of Zn_{ads}, as well as two mixtures of complexes on quartz and $SiO_{2(am)}$, thus serving as an ideal system for interrogating Zn adsorption complex differentiation with XANES spectroscopy.

Inner-sphere Zn complexation on the surface of silica has been shown to occur as a monodentate structure that locally passivates two reactive surface sites and releases two protons to maintain charge balance with the single bond of a divalent cation to the mineral surface (Nelson *et al.*, 2018). As such, the Zn *K*-edge XANES spectra of tetrahedral and octahedral inner-sphere adsorption complexes at the silica–water interface portray the electronic environment of Zn with three and five water ligands, respectively, and a silica surface ligand (Zn–O–Si). Therefore, the XANES spectra are dominated by the bonding energetics of Zn attached to waters of hydration, and the impacts of the direct bond to the surface are subtler in expression within XANES spectra. For these reasons it is not surprising that the XANES spectra of Zn adsorption complexes on silica most closely resemble that of aqueous Zn, though spectral complexity persists from bonding to the underlying silica surface (compare Figs. 1–4). The examination of standards and samples by peak absorbance in XANES spectra and absorption-edge energies clearly shows that Zn adsorbed to silica follows a trend between Zn silicate minerals (*i.e.* willemite and hemimorphite) and aqueous Zn (Fig. 5). For comparison, the single XANES spectrum denoted as Zn sorbed to a high-surface-area amorphous silica gel by Hamilton *et al.* (2016) more closely resembles the spectrum of willemite in their work, as well as in this study, compared with the spectra of Zn adsorbed to silica in this study, potentially attributable to the presence of a Zn silicate surface precipitate rather than an adsorbed complex on the silica gel material, which is less similar to natural silica materials than those examined herein (Nelson *et al.*, 2017, 2018; Zhuravlev, 2000).

As Zn–O coordination of Zn_{ads} shifts from dominantly octahedral to dominantly tetrahedral, the Zn *K*-edge XANES absorbance peak intensity decreases and differentiates. The chemical change in adsorption complexes at the silica surface amounts to fewer waters of hydration surrounding adsorbed Zn, such that the Zn–O bonds with water molecules decrease in proportion relative to the Zn–O bond with the silica surface. As tetrahedral Zn_{ads} complexes dominate, the leading local maximum absorbance peak becomes apparent and is similarly positioned at an energy level compared with the peak intensity seen in the XANES spectra for Zn silicate minerals with Zn in tetrahedral coordination (*i.e.* willemite and hemimorphite) and the leading absorbance peak of Zn oxide (*i.e.* zincite). The energy space between the two absorbance peak features of the XANES *K*-edge is 2.4 eV for Zn on quartz (Fig. 3) and 3.2 eV for Zn on $SiO_{2(am)}$ (Fig. 4). This *K*-edge peak feature of two local maxima observed for tetrahedral Zn_{ads} on silica is also present in the XANES spectrum of tetracoordinated Zn^{2+} within a SiO_2 catalyst (Schweitzer *et al.*, 2014), supporting the fingerprinting capability of this XANES spectral feature. The normalized absorbance peak intensity is also slightly lower for Zn complexes adsorbed to amorphous silica compared with quartz, posited to result from Zn adsorbed to the disordered silica surface [$SiO_{2(am)}$] residing slightly closer to the mineral surface with shorter Zn–O bonds than Zn adsorbed to quartz (Nelson *et al.*, 2017), which leads to a larger proportional contribution of the surface interactions over Zn–H_2O interactions to electronic distribution represented in the XANES spectra of Zn on $SiO_{2(am)}$ than quartz.

LCF of samples was used to explore quantitative identification of Zn surface complex type and sensitivity of XANES spectroscopy to changes in Zn adsorption geometry. Although the Zn coordination environment of these adsorption complexes is known from EXAFS spectral investigation, the degree to which XANES spectral features are uniquely identifiable, distinct and directly relatable to complex geometry must be assessed. Such distinguishability impacts the interchangeability of lone Zn adsorption samples to be used as standards representing Zn sorption when determining the composition of natural samples with LCF. For $SiO_{2(am)}$, LCF of the XANES spectrum of a mixture of Zn adsorption complexes (LCF of Am2 by Am1 and Am3) identified the composition as nearly equivalent proportions of tet-IS Zn_{ads} and oct-IS Zn_{ads} (Table 2 and Figs. 4 and S1). For quartz, LCF of the XANES spectrum of a mixture of Zn adsorption complexes (LCF of Qtz2 by Qtz1, Qtz3 and/or Qtz4) identified the composition as dominantly tet-IS Zn_{ads} (Table 2 and Figs. 4 and S1). Based on all fits, the remainder is attributable to octahedral coordination (Table 2 and Fig. S1). The fit with the smallest reduced chi-squared attributes the remainder of surface complexes to a reservoir of oct-OS Zn_{ads} and a separate reservoir, approximately one-third in size, of oct-IS Zn_{ads} (Table 2). However, the increase in error on individual proportions of each type of complex does not justify the use of three standards over two for the very small reduction in goodness of fit as assessed by reduced chi-squared (Table 2). Thus, LCF of Zn adsorption complexes on sample Qtz2 distributes Zn as majority tet-IS Zn_{ads} and a remainder nearly fully comprised of oct-OS Zn_{ads}, which aligns well with the expectation from previous EXAFS spectral analysis of this particular sample (Nelson *et al.*, 2017). Importantly, this LCF analysis of Zn *K*-edge XANES spectra of Zn_{ads} on silica as mixtures of tetrahedral and octahedral complexes demonstrates the feasibility of deciphering proportions of Zn sorbed species in different coordination environments when sorption endmembers are known and their XANES spectra are distinct enough from one another.

3.3. Implications for XANES analysis of Zn_{ads} in other systems

These XANES results for Zn_{ads} on silica highlight the use of XANES analysis for identification of the first-shell O coordination environments of Zn adsorption complexes and warrant similar investigation in other metal-ion–mineral systems. For example, XANES experimentation and modeling of Zn sorbed on ferrihydrite has been harnessed to add understanding to EXAFS analysis of the system (Waychunas *et al.*, 2003) but could be expanded for deeper interrogation of unknown surface speciation in controlled sorbed systems as carried out herein. A database of XANES spectra from more sorption systems may also foster benchmarking of three-dimensional stereochemical analysis via XANES model calculations, such as conducted for arsenate adsorption onto TiO_2 surfaces for which reduction in absorbance could be attributed to structural disorder (He *et al.*, 2012). Similar modeling of the XANES spectra of Zn_{ads} on silica presented here may elucidate the underlying cause of the diagnostic *K*-edge features for which these samples serve to benchmark.

Furthermore, although XANES analysis has been used in examining Zn speciation, such as in smelter-affected boreal-forest soil samples with reference spectra that included Zn adsorbed to smectite, goethite, birnessite and an amorphous silica gel (Hamilton *et al.*, 2016), the Zn adsorption standards are often not under focus and are taken to be comprised themselves of a single species with a singular coordination environment. The XANES examination of Zn adsorbed to quartz and $SiO_{2(am)}$ presented herein suggests that complexities in surface adsorption complexes manifest in XANES spectra, and thus need thorough investigation before using sorption standards in LCF speciation tests of natural samples. Differences seen in XANES spectra of Zn adsorbed to goethite used as standards for deciphering the speciation of Zn in natural samples exemplify this. Isotopic and EXAFS analyses illustrate that Zn on iron oxides resides in multiple coordination environments determined by surface coverage and reaction time (Nachtegaal & Sparks, 2004; Ha *et al.*, 2009; Juillot *et al.*, 2008); however, a single Zn_{ads} on goethite sample was used to represent the case for Zn sorption on goethite in the works of Hamilton *et al.* (2016) and Mamindy-Pajany *et al.* (2014). One sorption standard of Zn_{ads} on goethite used in XANES LCF is ascribed to octahedral coordination based on corresponding EXAFS analysis and contains a single *K*-edge peak feature (Hamilton *et al.*, 2016), whereas the other Zn_{ads} on goethite sorption standard presents two spectral peak features in the *K*-edge peak (Mamindy-Pajany *et al.*, 2014). This difference in the Zn_{ads} on goethite XANES spectra is similar to the difference in single and double *K*-edge peak spectral features of Zn_{ads} on silica seen in this work that correspond to octahedral and tetrahedral coordination, respectively. The two Zn_{ads} on goethite XANES spectra may represent an instance where the Zn_{ads} on goethite of Mamindy-Pajany *et al.* (2014) is in a different coordination compared with that of Hamilton *et al.* (2016). The natural samples examined therein may contain complexities in the set of adsorbed species that are not fully represented by one of the different Zn_{ads} on goethite XANES standards, thus leading to potentially erroneous attribution of a Zn reservoir within the sample to a specific complex when multiple or another are present.

In addition to establishing the presence of particular sorbed species, understanding the persistence of surface-bound metal ions in dynamic natural environments is important and related to the relationship between bond length and bond strength. The shorter bonds of tetrahedral Zn_{ads} on silica (average Zn–O bond distance of 1.94–1.97 Å) compared with octahedral Zn_{ads} on silica (average Zn–O bond distance of 2.04–2.07 Å) align with stronger binding to the surface (Nelson *et al.*, 2017, 2018), analogous to the case of tetrahedral over octahedral triple-corner-sharing Zn surface complexes on birnessite (Kwon *et al.*, 2009). These tetrahedral Zn_{ads} species may therefore be less labile under changing geochemical conditions than their octahedral counterparts. Thus, the ability to use the observation of two versus one *K*-edge peak features as a diagnostic for tetrahedral versus octahedral Zn_{ads} on silica, respectively, may enable inferences about sorbed Zn mobility in natural systems from XANES analysis, particularly at lower concentrations than required for EXAFS investigation.

4. Conclusions

Zinc *K*-edge XANES spectral analysis of Zn adsorbed to quartz and amorphous silica [$SiO_{2(am)}$] reveals that sorption complex geometry and underlying surface disorder manifest in XANES spectra. Differences in the Zn coordination environment are distinguishable in Zn *K*-edge XANES spectra, where peak absorbance and absorption-edge energy position generally decrease with increasing surface disorder and decreasing Zn–O coordination. The XANES spectral differences between the five endmembers of Zn adsorption complexes at the silica–water interface [outer-sphere octahedral Zn_{ads} on quartz, inner-sphere octahedral Zn_{ads} on quartz, inner-sphere tetrahedral Zn_{ads} on quartz, inner-sphere octahedral Zn_{ads} on $SiO_{2(am)}$ and inner-sphere tetrahedral Zn_{ads} on $SiO_{2(am)}$] at circumneutral pH illustrate that use of only one Zn_{ads} standard on a particular mineral surface may not capture diagnostic XANES spectral features from sorbed Zn to that mineral in natural samples. The deciphering of Zn adsorption complex mixtures with well characterized endmembers that present dependencies on coordination environment and surface disorder calls for further work in more metal-ion–mineral–water systems to identify diagnostic XANES spectral features of sorption complexes. To the degree that correlations between XANES spectral features and adsorption complex geometries are known, inferences might be made from XANES spectra of natural samples where concentrations are lower than requisite for direct EXAFS analysis of coordination environments.

Acknowledgements

The author thanks John Bargar for guidance at SSRL, Kate Maher for helpful discussions and Guangchao Li for ICP-OES laboratory support.

Funding information

This study was supported by the US National Science Foundation under Grant No. DGE-1147470. Use of the SSRL, SLAC National Accelerator Laboratory, is supported by the US Department of Energy, Office of Science, Office of Basic Energy Sciences under Contract No. DE-AC02-76SF00515.

References

Al-Ebraheem, A., Goettlicher, J., Geraki, K., Ralph, S. & Farquharson, M. J. (2010). *X-ray Spectrom.* **39**, 332–337.
Anderson, P. R. & Benjamin, M. M. (1990). *ACS Symp. Ser.*, **416**, 272–281.
Bazin, D., Carpentier, X., Brocheriou, I., Dorfmuller, P., Aubert, S., Chappard, C., Thiaudière, D., Reguer, S., Waychunas, G., Jungers, P. & Daudon, M. (2009). *Biochimie*, **91**, 1294–1300.
Brugger, J. L., Liu, W., Etschmann, B., Mei, Y., Sherman, D. M. & Testemale, D. (2016). *Chem. Geol.* **447**, 219–253.
Castorina, E., Ingall, E. D., Morton, P. L., Tavakoli, D. A. & Lai, B. (2019). *J. Synchrotron Rad.* **26**, 1302–1309.
Coston, J. A., Fuller, C. C. & Davis, J. A. (1995). *Geochim. Cosmochim. Acta*, **59**, 3535–3547.
Davis, J. A., Coston, J. A., Kent, D. B. & Fuller, C. C. (1998). *Environ. Sci. Technol.* **32**, 2820–2828.
Ellwood, M. J. & Hunter, K. A. (2000). *Limnol. Oceanogr.* **45**, 1517–1524.
Guinoiseau, D., Gélabert, A., Moureau, J., Louvat, P. & Benedetti, M. F. (2016). *Environ. Sci. Technol.* **50**, 1844–1852.
Ha, J., Farges, F. & Brown, G. E. Jr (2007). *AIP Conf. Proc.* **882**, 238–240.
Ha, J., Trainor, T. P., Farges, F. & Brown, G. E. Jr (2009). *Langmuir*, **25**, 5574–5585.
Hamilton, J. G., Farrell, R. E., Chen, N., Feng, R., Reid, J. & Peak, D. (2016). *J. Environ. Qual.* **45**, 684–692.
He, G., Pan, G. & Zhang, M. (2012). *J. Synchrotron Rad.* **19**, 394–399.
Juillot, F., Maréchal, C., Ponthieu, M., Cacaly, S., Morin, G., Benedetti, M., Hazemann, J. L., Proux, O. & Guyot, F. (2008). *Geochim. Cosmochim. Acta*, **72**, 4886–4900.
Kwon, K. D., Refson, K. & Sposito, G. (2009). *Geochim. Cosmochim. Acta*, **73**, 1273–1284.
Lee, S., Anderson, P. R., Bunker, G. B. & Karanfil, C. (2004). *Environ. Sci. Technol.* **38**, 5426–5432.
Liu, Y.-C., Wang, Q. & Lu, L.-H. (2003). *Chem. Phys. Lett.* **381**, 210–215.
Mamindy-Pajany, Y., Sayen, S., Mosselmans, J. F. W. & Guillon, E. (2014). *Environ. Sci. Technol.* **48**, 7237–7244.
Manceau, A., Lanson, B. & Drits, V. A. (2002). *Geochim. Cosmochim. Acta*, **66**, 2639–2663.
Martínez, C. E., Bazilevskaya, K. A. & Lanzirotti, A. (2006). *Environ. Sci. Technol.* **40**, 5688–5695.
Migliorati, V., Zitolo, A., Chillemi, G. & D'Angelo, P. (2012). *ChemPlusChem*, **77**, 234–239.
Nachtegaal, M. & Sparks, D. L. (2004). *J. Colloid Interface Sci.* **276**, 13–23.
Nelson, J., Bargar, J. R., Wasylenki, L., Brown, G. E. Jr & Maher, K. (2018). *Geochim. Cosmochim. Acta*, **240**, 80–97.
Nelson, J., Wasylenki, L., Bargar, J. R., Brown, G. E. Jr & Maher, K. (2017). *Geochim. Cosmochim. Acta*, **215**, 354–376.
Osaki, S., Miyoshi, T., Sugihara, S. & Takashima, Y. (1990). *Sci. Total Environ.* **99**, 105–114.
Qin, Z., Yin, H., Wang, X., Zhang, Q., Lan, S., Koopal, L. K., Zheng, L., Feng, X. & Liu, F. (2018). *Appl. Clay Sci.* **161**, 169–175.
Ravel, B. & Newville, M. (2005). *J. Synchrotron Rad.* **12**, 537–541.
Roberts, D. R., Ford, R. G. & Sparks, D. L. (2003). *J. Colloid Interface Sci.* **263**, 364–376.
Rouff, A. A., Eaton, T. T. & Lanzirotti, A. (2013). *Chemosphere*, **93**, 2159–2164.
Sandstead, H. H. (2014). *Handbook on the Toxicology of Metals*, 4th ed., pp. 1369–1386. Elsevier.
Schweitzer, N. M., Hu, B., Das, U., Kim, H., Greeley, J., Curtiss, L. A., Stair, P. C., Miller, J. T. & Hock, A. S. (2014). *ACS Catal.* **4**, 1091–1098.
Sverjensky, D. A. (1993). *Nature*, **364**, 776–780.
Thomas, S. A., Mishra, B. & Myneni, S. C. B. (2019). *J. Phys. Chem. Lett.* **10**, 2585–2592.
Trainor, T. P., Brown, G. E. Jr & Parks, G. A. (2000). *J. Colloid Interface Sci.* **231**, 359–372.
Veiga, J. P. & Figueiredo, M. O. (2008). *X-ray Spectrom.* **37**, 458–461.
Waychunas, G. A., Fuller, C. C. & Davis, J. A. (2002). *Geochim. Cosmochim. Acta*, **66**, 1119–1137.
Waychunas, G. A., Fuller, C. C., Davis, J. A. & Rehr, J. J. (2003). *Geochim. Cosmochim. Acta*, **67**, 1031–1043.
Webb, S. M. (2005). *Phys. Scr.* **T115**, 1011–1014.
Zhuravlev, L. T. (2000). *Colloids Surf. A Physicochem. Eng. Asp.* **173**, 1–38.